

RESEARCH ARTICLE | JULY 11 2013

# Atomic data for beam-stimulated plasma spectroscopy in fusion plasmas

O. Marchuk; Yu. Ralchenko; D. R. Schultz; W. Biel; T. Schlummer; TEXTOR-team



*AIP Conference Proceedings* 1545, 153–163 (2013)

<https://doi.org/10.1063/1.4815849>



CrossMark

05 July 2023 11:10:42

## AIP Advances

Why Publish With Us?

-  **25 DAYS**  
average time to 1st decision
-  **740+ DOWNLOADS**  
average per article
-  **INCLUSIVE**  
scope

[Learn More](#)



# Atomic data for beam-stimulated plasma spectroscopy in fusion plasmas

O. Marchuk<sup>a</sup>, Yu. Ralchenko<sup>b</sup>, D.R. Schultz<sup>c</sup>, W. Biel<sup>a</sup>, T. Schlummer<sup>a</sup> and the TEXTOR-team<sup>a</sup>

<sup>a</sup>*Institute of Energy and Climate Research, Forschungszentrum Jülich, 52425 Jülich, Germany*

<sup>b</sup>*Quantum Measurement Division, National Institute of Standards and Technology, Gaithersburg, MD 20899-8422, USA*

<sup>c</sup>*Department of Physics, University of North Texas, Denton, TX 76203, USA*

## Abstract.

Injection of high energy atoms into a confined plasma volume is an established diagnostic technique in fusion research. This method strongly depends on the quality of atomic data for charge-exchange recombination spectroscopy (CXRS), motional Stark effect (MSE) and beam-emission spectroscopy (BES). We present some examples of atomic data for CXRS and review the current status of collisional data for parabolic states of hydrogen atoms that are used for accurate MSE modeling. It is shown that the collisional data require knowledge of the excitation density matrix including the off-diagonal matrix elements. The new datasets for transitions between parabolic states are used in an extended collisional-radiative model. The ratios between the  $\sigma$ - and  $\pi$ -components and the beam-emission rate coefficients are calculated in a quasi-steady state approximation. Good agreement with the experimental data from JET is found which points out to strong deviations from the statistical distribution for magnetic sublevels.

**Keywords:** atomic data, charge-exchange, atom-ion collisions, Stark effect, density matrix

**PACS:** 52.25.Xz, 52.20.Hv, 32.60.+i, 32.70.Fw, 32.30.Jc

## INTRODUCTION

Plasma heating by injection of highly-energetic hydrogen or deuterium atoms with the energy of  $E=(20 \text{ to } 500) \text{ keV/u}$  has become one of the most promising tools to approach ignition conditions in magnetic fusion [1]. Fast ionized atoms provide particle, momentum and heat transfer through binary collisions with other plasma particles, primarily ions. Hence, a deep understanding of beam propagation in a plasma is important for successful operation of the new generation of fusion devices. On the other hand, rich spectroscopic signatures of beam interaction with plasma constituents brought about a rapid development of new diagnostic methods for fusion. Local measurements of concentrations of impurities, magnetic fields, and radial distributions of fast ions are only a few examples of beam diagnostic applications [2].

Most of spectroscopic information in beam diagnostics is derived from the following atomic processes:

$$X^{z+1} + H_0 \rightarrow X^{z*} + H^+ \rightarrow h\nu, \quad (1)$$

$$H_0 + (H^+, X^{z+1}, e) \rightarrow H^* + (H^+, X^{z+1}, e) \rightarrow h\nu, \quad (2)$$

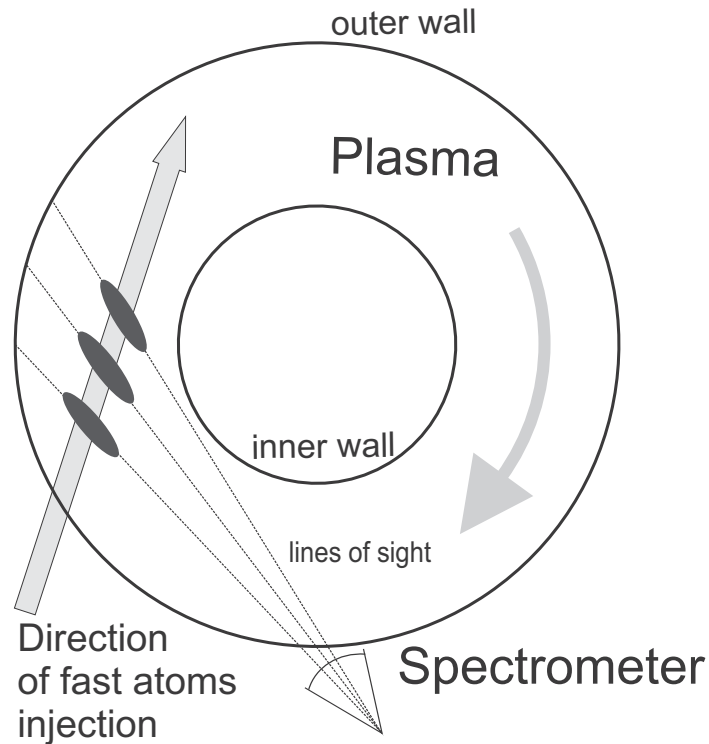


**FIGURE 1.** Top view of the injection scheme in tokamak plasmas. Zones of beam emission and charge exchange emission observed by a spectrometer are shown as grey spots at the intersection of the lines of sight and beam direction. The spectral line emission can be separated from the passive edge emission due to the Doppler shift.

where emitted photons in (1) originate from the impurity ions  $X^Z$  due to radiative stabilization of the excited state  $X^{Z*}$ , and in (2) the observed photons are emitted by the fast hydrogen atoms  $H^*$ . These measurements are usually performed in the visible spectral range, taking advantage of high spectral resolution required for Doppler shift and ion temperature measurements, relatively simple absolute calibration technique, and high throughput of the optical system. Figure 1 shows a typical observation scheme in fusion devices. The fast atoms are injected from the outer wall of the plasma vessel and different lines of sight provide the required spatial resolution of measurements.

Emission of spectral lines is often distorted by the presence of the so-called passive, or cold, component emitted at the plasma edge. Only the charge-exchange (CX) lines from high Rydberg states of intermediate and high  $z$  impurity ions are free from such blending. The active signal is Doppler shifted relative to the passive one. In case of reaction (1) the Doppler shift is sustained due to plasma rotation, and in (2) it exists due to high beam velocity and energy  $E \gg T$  where  $T$  is the plasma temperature.

## ATOMIC DATA FOR CHARGE EXCHANGE DIAGNOSTICS

For the majority of spectroscopic observations, the atomic data required to derive concentration of impurity ions can be represented as the *effective emission rate coefficients*  $Q_{eff}^{cx}$ . In this case, the intensity of a spectral line between the principal quantum numbers  $n_1$  and  $n_2$  can be written as:

$$I_{cx}(n_1 \rightarrow n_2) \propto N_b N_{z+1} Q_{eff}^{cx}, \quad (3)$$

where  $N_b$  is the beam density in the ground state and  $N_{z+1}$  is the concentration of the impurity ions  $X^{z+1}$ . The Doppler broadening of these lines exceeds the fine structure splitting by orders of magnitude so that only the rate coefficients between the principal quantum numbers are required.

Calculation of the rate coefficients involves two steps. First, the CX cross sections  $\sigma_{nl}$  resolved over the principal  $n$  and orbital  $l$  quantum numbers are to be determined. Then, the relative excited level populations  $p_{nl} = N_{nl}/N_0$  (here  $N_{nl}$  and  $N_0$  are the densities of the excited and ground states, respectively) are calculated within a collisional-radiative (CR) model [3]. The rate coefficients are then obtained according to the following formula:

$$Q_{eff}^{cx}(n_1 \rightarrow n_2) = \sum_{l_1=0}^{n_1-1} \sum_{l_2=0}^{n_2-1} p_{n_1 l_1} A_{n_1 l_1 \rightarrow n_2 l_2}, \quad (4)$$

where  $A_{n_1 l_1 \rightarrow n_2 l_2}$  is the radiative transition probability between configurations  $n_1 l_1$  and  $n_2 l_2$ , and  $p_{n_1 l_1}$  is the population of the upper level of the corresponding transitions.

Significant progress was achieved in the calculation of effective CX rate coefficients and CR modeling for impurities with low  $z$  numbers, such as helium, beryllium or carbon [4, 5]. The first CR models were based on  $n$  states only, assuming statistical distribution for the orbital quantum numbers  $l$ . Today most CR models are resolved over both quantum numbers, and the statistical assumption is not longer needed [6]. For impurities with intermediate  $z$  values, such as argon, the situation is still unsettled. The partial CX cross sections  $\sigma_{nl}$  significantly vary for different calculations, and experimental cross sections for such H-like impurities are still very rare. Indeed, the  $nl$ -resolved cross sections differ by an order of magnitude and the total CX cross section deviates by a factor of two among different calculations [7, 8, 9]. In addition to this, CR models are to be extended to high  $n$  without assumption of statistical redistribution for  $\Delta n = 0$ . Our collisional-radiative model was extended up to  $n=30$  with the goal to produce effective rate coefficients and to analyze the impact of cascades on the CX lines of argon. The details of calculations could be found in [10, 13]. The  $nl$ -resolved CX cross-sections were taken from [7, 8].

Figure 2 shows the calculated effective rate coefficients for H-like argon [10, 11, 12, 13]. These calculations show a significant effect of radiative cascades on the resulting effective rate coefficient for the visible  $n=16 \rightarrow n=15$  CX line to be used in ITER diagnostics. Account of the  $n \leq 30$  states is seen to result in a 30-40% increase in the rate coefficients as compared to the  $n \leq 16$  calculations. The results converge starting from  $n \approx 25$ . The ADAS calculations are also shown for comparison. Good agreement between

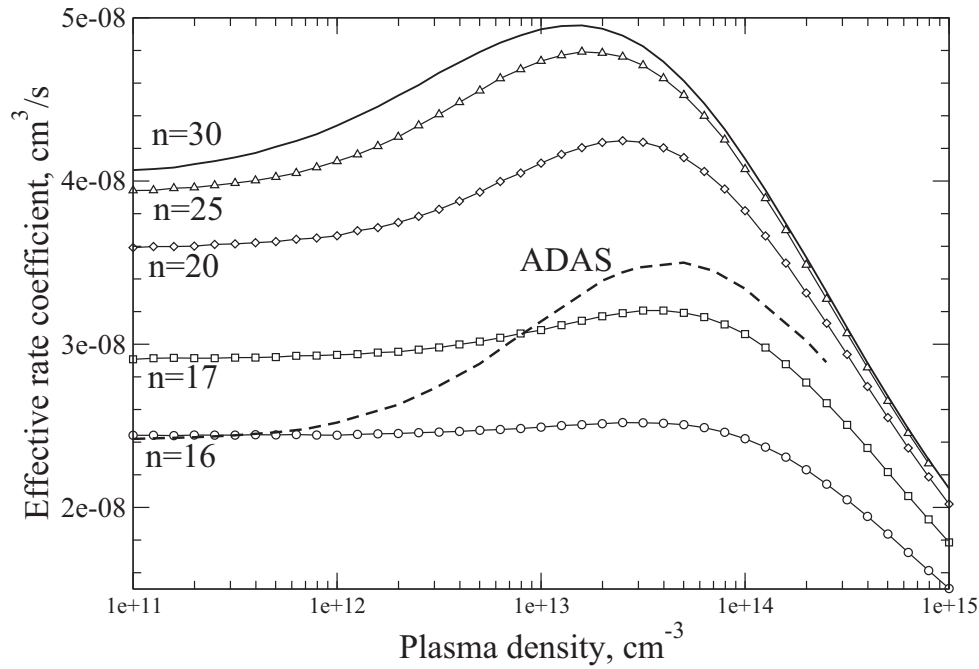


**FIGURE 2.** Effective CX rate coefficients for the transition  $n=16 \rightarrow n=15$  in H-like argon. The beam energy is 70 keV/u, the plasma temperature is 2 keV. The collisional radiative model was limited by  $n_{max}=16, 17, 20, 25$  and 30. The effective rate coefficients from the ADAS database are also presented for comparison[12].

our calculations and ADAS results is established only at low plasma density where our model was limited to  $n \leq 16$ . Inclusion of higher principal quantum numbers leads to stronger deviations as the effective rate coefficients become larger in our calculations. Verification of cross sections and effective rate coefficients remains a challenging task in plasma research. New insights on the quality of the partial and total CX cross sections can be obtained for these H-like impurities using combination of X-ray and visible spectroscopy which are foreseen in the near future.

## ATOMIC DATA FOR MSE AND BES DIAGNOSTICS

Similar to the CX spectroscopy, extensive atomic data are required to perform diagnostic analysis for the beam-emission spectroscopy. Here the major parameters include populations of excited states, line intensities, and beam attenuation characteristics. Unlike other laboratory plasmas, calculation of atomic data relevant to the excited states of hydrogen atoms in the beam is not straightforward. The atoms penetrating the confining magnetic field are subject to the linear Stark effect with the induced electric field  $F = v \times B$  where  $v$  is the beam velocity and  $B$  is the magnetic field strength. Consequently, the eigenstates of the beam atoms are in fact the *parabolic* states that are characterized, in addition to  $n$ , by the electric  $k$  and magnetic  $m$  numbers [14]. This feature greatly complicates calculation of collisional data needed for beam diagnostics.

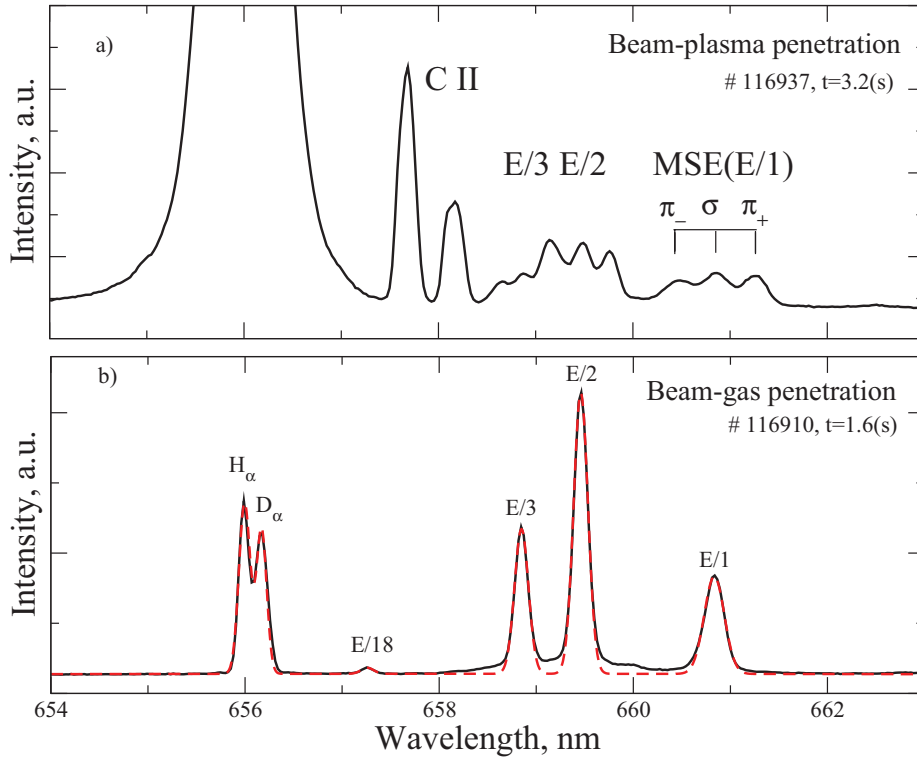


**FIGURE 3.** Example of the beam emission spectra measured from the tokamak TEXTOR. Figure a) shows the complex structure of the Stark effect spectra from the major, second and the third energy components of the hydrogen beam. Figure b) shows a relatively simple spectrum of the injection of the beam atoms into the torus filled with gas. The acceleration energy was in both cases equals to 55 keV. In a) the magnetic field was 2.55 T and in b) no magnetic field is applied and the gas pressure was 3mbar. The theoretical spectrum is shown in b) with red dashed line.

The MSE spectra are exemplified here by the recent beam-emission measurements from the TEXTOR tokamak. Figure 3(a) shows the spectra near the  $H_{\alpha}$  line during steady-state plasma operation, and Fig. 3(b) presents similar spectra in the torus filled with a gas without a magnetic field. In the former case, a strong unshifted  $D_{\alpha}$  line is accompanied by Stark multiplet emission for the major, second and third beam energy components. The C II edge lines are also present in the measured spectra. The  $\sigma$  and  $\pi$  components could only be resolved for the major energy component. The beam-gas spectrum of Fig. 3(b) does not exhibit any Stark splitting. The Doppler shifted spectral lines in this spectrum provide valuable information on the energy distribution between beam components and thus the energy transfer to plasma particles.

Any realistic approach to calculation of the MSE component spectra has to take into account the already mentioned fact that the eigenstates of hydrogen (or deuterium) under MSE conditions are the parabolic states. This affects both the atomic structure and the collisional calculations. Calculation of the energy levels, radiative transitions probabilities, and ionization rates can be easily performed within the perturbation theory. The collisional data such as the electron- and ion-impact cross sections for transitions between parabolic states are not available in the literature.

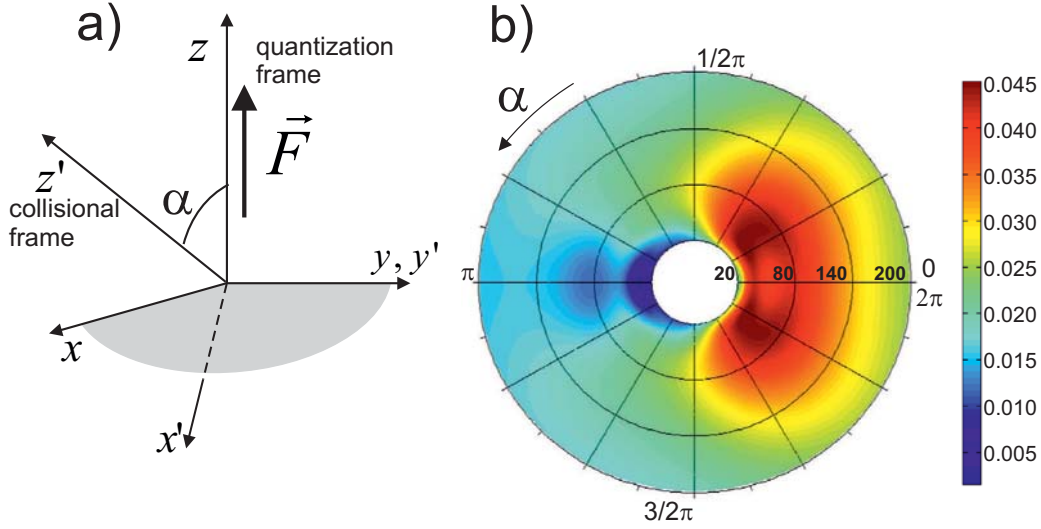


**FIGURE 4.** Collisional atomic data in parabolic representation. a) Transformation between the spherical and parabolic wavefunctions. b) Cross section of excitation from the ground state to the state (3,1,1) [18]. The polar angle is the angle  $\alpha$  between the electric field and the beam velocity. The radial axis is the collision energy in keV/u. The cross section is in units of  $\pi a_0^2$  where  $a_0$  is the Bohr radius.

The first models for the Stark effect in fusion plasmas used collisional data calculated in the Born approximation [15, 16]. However, for the beam energies below 200 keV/u, this high-energy method has inferior accuracy as compared to more sophisticated methods. Even the most advanced non-perturbative techniques are to be modified to account for the parabolic nature of atomic eigenstates under MSE conditions. A new general method was developed in Refs. [17, 18] and is briefly described here. The major difficulty in calculation of collisional characteristics is due to presence of two independent quantization axis. The direction of the electric field defines quantization axis  $z$  for the parabolic states of the beam atom (Fig. 4(a)). In a general collisional problem the quantization axis is normally chosen along the projectile velocity  $z'$ . For MSE, the angle between axis  $z$  and  $z'$  is  $\alpha = \pi/2$  as  $F = v \times B$ . We note that the collisional frame could always be chosen so that the axis  $y$  and  $y'$  coincide. The parabolic wavefunctions defined along the axis  $z$  can be represented as a linear combination of the spherical wavefunctions defined along the axis  $z'$  using the following expansion:

$$\Psi_{nkm} = \sum_{l=|m|}^{n-1} C_{nk}^{lm} \sum_{m'=-l}^l d_{lm'}^{m'}(\alpha) \phi_{nlm'}, \quad (5)$$

where  $\hat{C}$  is the matrix of Clebsch-Gordan coefficients [19] and  $\hat{d}$  is the quantum mechanical matrix of rotation [20]. This simple unitary transformation between wavefunctions allows one to calculate cross sections between the parabolic states using any standard method of collisional theory:

$$\sigma_{ab} = \frac{k_f}{k_i} \int |F_{ab}(\mathbf{q})|^2 d\mathbf{q}, \quad (6)$$

where  $F_{ab}$  is the scattering amplitude between the parabolic states  $a = n_a k_a m_a$  and  $b = n_b k_b m_b$ ,  $\mathbf{q} = \mathbf{k}_i - \mathbf{k}_f$  is the vector of momentum transfer and  $\mathbf{k}_i$  and  $\mathbf{k}_f$  are the momenta of the projectile before and after collision. It follows from Eq. (6) that the cross sections between parabolic states could be represented as the linear combinations of the cross sections between spherical wavefunctions and the off-diagonal elements of the collisional density matrix.

In a general case of an arbitrary angle  $\alpha$  between the electric field and projectile velocity (e.g., collisions between hydrogen in an electric field and incoming particles) the cross sections exhibit strong dependence on  $\alpha$ . Figure 4(b) presents an example of an excitation cross section from the H ground state to one of the parabolic state of  $n=3$  levels, where the AOCC calculations [21] for the density matrix elements were used [18]. The strong  $\alpha$ -dependence appears due to the presence of the coherent term  $s$ - $d$  in the expansion of the cross section. This term, as in case of the  $s$ - $p$  coherence [22] for  $n=2$  excitation, disappears when  $\alpha$  increases from 0 to  $\pi/2$ . Note also that the dependence of the cross section on orientation between the direction of the projectile and electric field was initially shown for transitions between high Rydberg states of atoms placed in an electric field [23, 24].

## LINE INTENSITIES OF MSE DIAGNOSTIC

The calculated atomic structure and collisional data were incorporated in the CR model NOMAD [25] that was extended to  $n \leq 10$  and used to determine the excited populations of the beam atoms, line intensities of the fine structure components, beam stopping power, and emission rate coefficients [18, 26]. One of the most important questions related to calculation of line intensities and other derived parameters is whether the statistical (Boltzmann) distribution can be used to calculate sublevel populations within a specific  $n$ . Unlike the statistical atomic models for beams in plasma [5, 27, 28], this new model provides populations of magnetic sublevels without any assumption on Boltzmann distribution. Figure 5 presents the reduced populations of the excited states  $n_i = N_i/g_i$  (here  $g_i$  is the statistical weight of a magnetic sublevel  $nkm$ ) for a typical fusion plasma with density  $3 \times 10^{13} \text{ cm}^{-3}$ , temperature 5 keV, magnetic field 5 T and beam energy 80 keV/u. The top panel (a) shows the results of calculation without electric-field-induced ionization. For the exact statistical distribution within a specific  $n$ , the populations  $n_i$  should have the same values. Obviously, this is not the case for  $n \leq 6$  with deviations of about 30-50%. Only the  $n=7$  sublevels approach the statistical equilibrium. The field ionization effect (bottom panel of Fig. 5) that must be included for strong magnetic fields destroys quasi-statistical distribution of populations even for the highest  $n=7$ . The populations of the  $n=5$  and  $n=6$  sublevels are also partially reduced and the deviation to the statistical picture also increases.

The non-statistical distribution of state populations has a considerable effect on the line ratios observed in experiments. Figure 6 presents comparison of the recent experimental data from JET as well as the results of NOMAD simulations [17, 29]. First, significant differences between the measurements and the statistical predications (horizontal lines) are obvious. The non-statistical calculations were performed using either a complete set of data calculated within the Glauber approximation (dashed lines) [30]

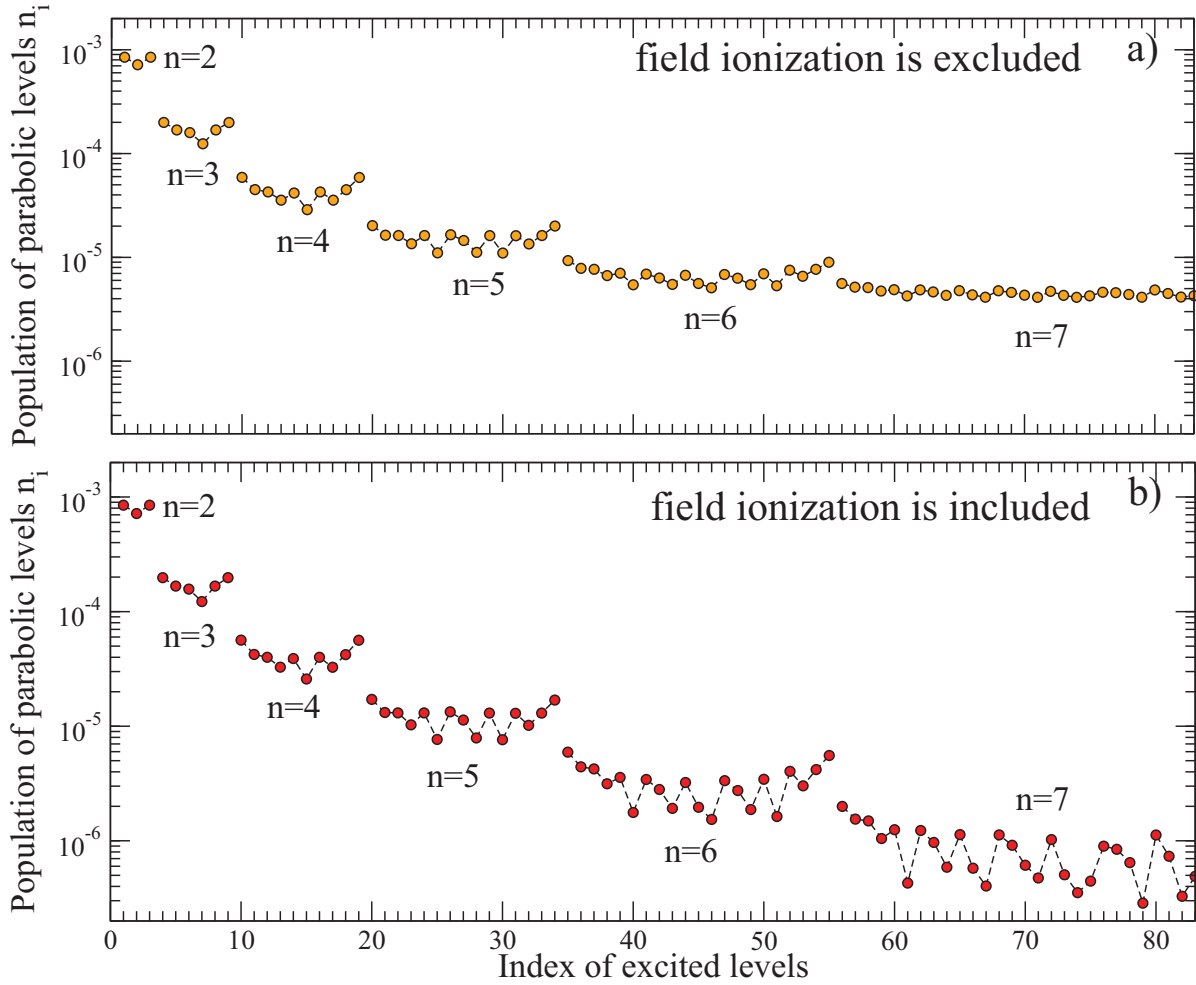


**FIGURE 5.** Reduced populations  $n_i$  of parabolic eigenstates of the beam. The beam energy is 80 keV/u, the plasma temperature is 5 keV, the magnetic field is 3 T and the plasma density is  $3 \cdot 10^{13} \text{ cm}^{-3}$ . a) Field ionization is excluded; b) field ionization is included. Populations of the states belonging to the same principal quantum number  $n$  are shown as solid circles connected by thin dashed line. The index of the states starts from the ground state (index is 0 and so on).

or Glauber + atomic-orbital-close-coupling (AOCC) combination of data (solid lines) [18]. A very good agreement between the Glauber approximation and the experimental data is clear. The model based on the AOCC excitation data to the  $n=2$  and  $n=3$  states shows some deviation from the experimental data, especially for the  $\pi_4$ -to- $\pi_3$  intensities. This emphasizes the necessity of further theoretical and experimental analysis of the proton-impact excitation cross sections [31].

## CONCLUSIONS

Extensive atomic data are required to support diagnostic measurements based on injection of a neutral beam into plasma. Here we addressed in detail two types of data, namely,

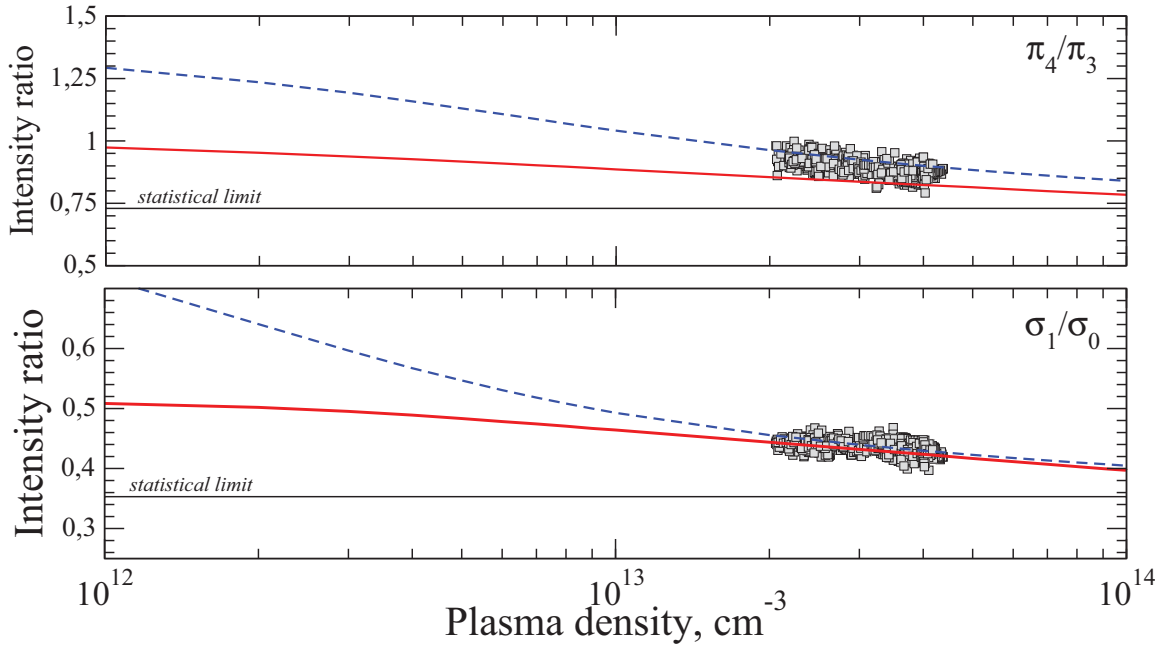


**FIGURE 6.** Measured and calculated ratio of the lines  $\pi_4/\pi_3$  and  $\sigma_1/\sigma_0$  [29]. Experimental data are shown as grey points, the results of calculation using only Glauber approximation [30] are blue dashed line, and the results of calculation using AOCC and Glauber approximations [18] are shown as red lines.

the effective charge-exchange rate coefficients and the collisional excitation data related to the motional Stark effect. The former are strongly affected by the uncertainties in the  $nl$  charge-exchange cross sections from ground or excited states of the beam. Extensive collisional-radiative models are required to handle the data up to  $n \approx 30$  in order to include radiative cascades from high Rydberg states. Simulations for H-like argon show that an increase of about 40% in the effective rates can be expected for more extensive models. The combined measurements of line emission using visible, XUV and x-ray spectroscopy seems to be the most promising tool to address this problem. The effect of the Zeeman-Stark splitting on the CX rate coefficients for low- $z$  impurities [3] also remains an unexplored domain. This problem will likely be addressed in the near future with introduction of new fusion devices operating with high magnetic fields.

The collisional excitation data, primarily due to heavy particle interactions, represent another important set of data for beam diagnostics. The Stark effect diagnostics or deposition of fast ions in a plasma crucially depend on populations of the excited states. Significant progress in understanding of beam emission was achieved in the last few years. The standard, or *statistical*, description of magnetic sublevel populations is being replaced by a detailed kinetic treatment of all physical processes affecting every parabolic *eigenstate* of the beam. The alignment between directions of the induced electric field and the beam velocity plays crucial role in calculation of the collisional cross sections that include coherent terms of the density matrix. The new time-dependent collisional-radiative model developed in [6, 29, 18, 26] incorporates all necessary atomic data to calculate populations of magnetic sublevels and provides Stark line intensities as

well as the beam emission and attenuation characteristics in a plasma. It is shown that the assumption on the statistical distribution within  $\Delta n = 0$  is not valid in the plasma, as confirmed by the numerous experiments at JET, ALCATOR C-Mod, TEXTOR, etc. A good agreement between the theoretical data using Glauber approximation and the experimental data from JET is obtained. The AOCC calculations are also very close to the experimental data, though a slight difference in  $\pi_4$ -to- $\pi_3$  lines ratio still exists. This emphasizes importance of further development of accurate methods for particle collisions under fusion plasma conditions.

## ACKNOWLEDGMENTS

The work of Yu.R. was supported in part by the Office of Fusion Energy Sciences of the U.S. Department of Energy. The authors are thankful to E. Stambulchik, G. Bertschinger, M. von Hellermann, and H.-J. Kunze for useful discussions.

## REFERENCES

1. Hemsworth R *et al.* *Nucl. Fusion* **49** 045006 (2009)
2. von Hellermann M *et al.*, *Rev. Sci. Instrum.* **T120** 19 (2005).
3. Fonck R J, Darrow D S and Jaehnig K P, *Phys. Rev. A* **29** 3288 (1984)
4. Minami T, Lee T-G, Pindzola M S and Schultz D R, *J Phys. B: At. Mol. Opt. Phys.* **41** 135201 (2008)
5. Summers H P, The ADAS User Manual (2004), version 2.6, <http://adas.phys.strath.ac.uk>
6. Marchuk O *et al.*, *J. Phys. B: At. Mol. Opt. Phys.* **42** 165701 (2009)
7. Schultz D R, Lee T-G and Loch S D, *J. Phys. B: At. Mol. Opt. Phys.* **43** 144002 (2010).
8. The Controlled Fusion Atomic Data Center, <http://www-cfadc.phy.ornl.gov/>
9. Errea L F *et al.*, *J. Phys. B: At. Mol. Opt. Phys.* **39** L91 (2006)
10. Schlummer T *et al.* APiP Conf. Proc., "Effective rate coefficients for charge-exchange on H-like helium and argon", Belfast, (2011)
11. Marchuk O *et al.*, ADAS Workshop, "Population kinetics of highly excited states of Ar XVIII", (2008)
12. OPEN-ADAS, [http://open.adas.ac.uk, /adf12/qef99#h/qef99#h\\_ornl#ar18.dat](http://open.adas.ac.uk, /adf12/qef99#h/qef99#h_ornl#ar18.dat) (2003)
13. Schlummer T., Diploma thesis, *Effektive Ratenkoeffizienten für die Ladungsaustauschspektroskopie an H-ähnlichem Argon* University of Cologne, Germany (2010)
14. Bethe H A and Salpeter E E, *Quantum Mechanics of One- and Two-Electron Atoms*, Plenum, New York, 1977, pp. 232-234, 276-278.
15. Gu M F, Holcomb C T, Jayakuma R J and Allen S L 2008 *J. Phys. B: At. Mol. Opt. Phys.* **41** 095701
16. Boileau A *et al.* 1989 *J. Phys. B: At. Mol. Opt. Phys.* **22** L145
17. Marchuk O *et al.*, AIP Conf. Proc, **1438** 169 (2011)
18. Marchuk O, Ralchenko Yu and Schultz D.R., *Plasma Phys. Contr. Fusion* **54** 095010 (2012)
19. Landau L D and Lifshitz E M, *Quantum Mechanics: Non-Relativistic Theory*, Pergamon, Oxford, 1976, p. 344.
20. Edmonds A R 1957 *Angular Momentum in Quantum Mechanics* (Princeton, NJ: Princeton University Press) p. 53
21. Kuang J and Lin C D, *J. Phys. B: At. Mol. Opt. Phys.* **29** 1207 (1996).
22. Eck T G 1973 *Phys. Rev. Lett.* **31** 270
23. Hickman A P 1985 *Phys. Rev. A* **28** 111
24. de Prunelé E, *Phys. Rev. A* **31** 3593 (1985).
25. Ralchenko Yu and Maron Y, *Quant. Spectr. Rad. Transf.* **71** 609 (2001).
26. Ralchenko Yu *et al.*, *Rev. Sci. Instrum.* **83** 10D504 (2012)
27. Marchuk O *et al.*, *Rev. Sci. Instrum.* **79** 10F532 (2008).

28. Hutchinson I H, *Plasma Phys. Control. Fusion* **44** 71 (2002).
29. Delabie E *et al.*, *Plasma Phys. Contr. Fusion* **52** 125008 (2010).
30. Marchuk O *et al.*, *J. Phys. B: At. Mol. Opt. Phys.* **43** 011002 (2010).
31. Schultz D R, Reinhold C O and Kristic P S 1997 *Phys Rev. Lett.* **78** 2720